Fuel 368 (2024) 131581

Contents lists available at ScienceDirect

Fuel

journal homepage: www.elsevier.com/locate/fuel

Full length article

Data-driven prediction of laminar burning velocity for ternary ammonia/hydrogen/methane/air premixed flames

Cihat Emre Üstün [a,*], Sven Eckart [b], Agustin Valera-Medina [c], Amin Paykani [a]

[a] School of Engineering and Materials Science, Queen Mary University of London, London, E1 4NS, United Kingdom
[b] Chair of Gas and Heat Technology, Institute of Thermal Engineering, Technische Universität Bergakademie Freiberg, Freiberg, 09599, Germany
[c] College of Physical Sciences and Engineering, Cardiff University, Cardiff, CF24 3AA, United Kingdom

ARTICLE INFO

Dataset link: https://github.com/cihatemreustunn/Ternaryblendsproject

Keywords:
Ammonia
Hydrogen
Methane
Machine learning
Laminar burning velocity

ABSTRACT

Zero-carbon fuels such as hydrogen and ammonia play a pivotal role in the energy transition by offering cleaner alternatives to natural gas (methane), especially in industrial combustion systems. Binary and ternary blends of these fuels offer a transitionary, low-carbon solution in the near future. Laminar burning velocity (LBV), as a fundamental combustion property, is significantly different for ammonia, hydrogen, and methane. Although the LBV of binary blends of these fuels is well-studied, ternary blends have not been extensively studied. In this study, the primary objective is to employ a simple ensemble learning method to predict the LBV of ternary ammonia/hydrogen/methane/air mixtures. The training dataset consists of experimental data sourced from a large number of publications (3,846 data points), as well as synthetic data generated by 1D freely propagating premixed flame simulations in Cantera using a detailed chemical kinetic model. Three machine learning algorithms, namely artificial neural networks, gaussian process regression, and extreme gradient boosting trees are trained and optimised. Then, a simple ensemble averaging method is used to reduce overfitting and improve robustness. The ensemble model achieves coefficient of determination (R^2) of 0.991 on the test set with an inference time that is approximately 8,000 times faster than the 1D simulation run time. The ensemble model is capable of predicting LBVs of ammonia/hydrogen/methane/air mixtures for T = [295–756 K], P = [1–10 bar], ϕ = [0.5–1.8] across all possible blending ratios.

1. Introduction

In the pursuit of achieving net-zero carbon emissions targets, future propulsion and power generation technologies are expected to incorporate low and zero-carbon energy fuels, coupled with advanced high-efficiency energy conversion devices [1,2]. Among the promising carbon-free fuels, ammonia (NH_3) stands out due to its high energy density and well-established production and distribution infrastructure [3]. However, as a fuel, NH_3 exhibits sub-optimal combustion properties, characterised by low burning velocity, a narrow flammability limit, high NO_x emissions, and a relatively high auto-ignition temperature. These limitations can be mitigated through the addition of hydrogen (H_2), which can be efficiently derived by partially cracking ammonia into H_2 and N_2 before the combustion process [4,5]. By blending NH_3 with H_2, the resulting NH_3/H_2 mixture demonstrates significantly improved flame stability and a higher burning velocity. Additionally, it was repeatedly reported that the NO_x emissions as low as 50 ppm are achievable with NH_3/H_2/air flames [3,6,7]. Research has shown that extremely lean NH_3/H_2/air mixtures hold strong potential for fuelling future internal combustion (IC) engines and gas turbines [8]. Moreover, the use of NH_3/H_2/air mixtures in gas turbines can enhance operational limits in comparison to the direct use of H_2/air as a fuel [9]. An additional advantage of using NH_3 is that H_2 can be derived from its pre-cracking process, providing a clear pathway for decarbonisation through the utilisation of NH_3/H_2 blends.

Ammonia is also expected to gradually displace natural gas (≈90% CH_4 in vol.) for power generation and heating applications [10]. Soot formation is another issue with incomplete combustion of HCs. It should be noted that NH_3 doping inhibits soot formation in CH_4 flames due to the chemical effect of NH_3 [11]. It was shown by Masoumi et al. [12] that increasing NH_3 content makes both NH_3/CH_4 and NH_3/H_2 flames more hydrodynamically stable due to flame thickening. Recent studies show a great interest in ternary blends of $NH_3/CH_4/H_2$/air [9,13–15]. Mashruk et al. [9] pointed out the pivotal role of $NH_3/CH_4/H_2$/air blends in the transition to the direct use of NH_3 and H_2 fuels in gas turbines and engines since reduced retrofitting would be required in the existing operational combustion devices.

* Corresponding author.
E-mail address: c.e.ustun@qmul.ac.uk (C.E. Üstün).

https://doi.org/10.1016/j.fuel.2024.131581
Received 20 December 2023; Received in revised form 13 March 2024; Accepted 21 March 2024
Available online 25 March 2024

Nomenclature

Abbreviations

$1D$	One-dimensional
ANN	Artificial neural network
$CART$	Classification and regression tree
DNN	Deep neural network
$GBDT$	Gradient boosting decision tree
GP	Gaussian process
GPR	Gaussian process regression
HC	Hydrocarbon
IC	Internal combustion
LBV	Laminar burning velocity
LBV	Mean absolute error
LBV	Root mean square error
ML	Machine learning
NTP	Normal temperature and pressure
RBF	Radial basis function
$ReLU$	Rectified linear unit activation function
$XGBoost$	Extreme gradient boosting trees

Symbols

α	Scale mixture
$\boldsymbol{\mu}$	Mean vector
$\boldsymbol{\theta_\mu}$	Mean vector hyperparameter
$\boldsymbol{\theta_k}$	Covariance matrix hyperparameter
$\boldsymbol{K}$	Covariance matrix
$\boldsymbol{X}$	Input matrix
$\boldsymbol{Y}$	Output matrix
ϵ_i	Initial temperature
γ	Regularisation hyperparameter 2
$\prime\prime\prime$	Length scale
$\mathcal{D}$	Dataset
$\mathcal{F}$	Collection of regression trees
$\mathcal{L}$	Objective function
$\Omega(f_k)$	Regularisation term
ϕ	Equivalence ratio
σ^2	Variance
O	Complexity
P_i	Initial pressure
R^2	Coefficient of determination
T_i	Initial temperature
X	Mole fraction

The operability maps of $NH_3/CH_4/H_2$/air mixtures under atmospheric conditions were produced. It was noted that the 30%–40% (vol.) H_2 addition caused flashback. Later, Berwal et al. [14] studied the LBV of $NH_3/CH_4/H_2$/air mixtures at elevated temperatures (300–750 K) for $\phi = 0.7-1.2$ and atmospheric pressure. The X_{NH_3} was varied between 0 and 30 in a CH_4/H_2 blend with 4:1 ratio. It was reported that a 7.2:1.8:1 ratio (vol. %) $CH_4/H_2/NH_3$/air mixture would reproduce adiabatic flame temperatures of natural gas (NG) with a slightly higher LBV while reducing CO and CO_2 emissions about 10%. Later, Yasiry et al. [15] carried out an experimental study to measure the LBV of $NH_3/CH_4/H_2$/air mixtures at normal temperature and pressure (NTP) conditions for $\phi = 0.8 - 1.2$. The X_{H_2} was varied between 0 and 40 in a CH_4/H_2 blend. Detailed chemical kinetic mechanisms were compared [16–18] and it was reported that the Li mechanism [18] provided the best LBV computation for ternary blends, increasing accuracy was observed with increased NH_3 content. More recently, Berwal et al. [13] investigated the LBV of ternary $NH_3/CH_4/H_2$/air blends at elevated temperature and pressure conditions, extending their previous work to 5 bar. It was noted that the LBV for the ternary mixtures would be comparable to that of CH_4/air at 5 bar. It was also stated that the Li [18] and Okafor [16] mechanisms were both comparable to the experimental measurements up to 5 bar. However, further works [19] have shown that additional improvement on current reaction mechanisms is critically required as models such as the latter can under/overpredict LBV and species consumption, particularly when evaluating ternary blends for which the mechanisms have been barely tried. Finally, this work demonstrated the practical feasibility of ternary $NH_3/CH_4/H_2$/air blends for the transition to low to zero-carbon combustion systems. In conclusion, $NH_3/CH_4/H_2$/air mixtures in current combustion units become a viable prospect, warranting an in-depth analysis of the stability, emissions, and flame characteristics of these ternary blends.

The recent progress in the field of machine learning (ML), coupled with the increasing volume of available data, progress in computing (GPU, TPU, cloud computing, edge computing), and data storage technologies for handling big data, offer promising applications in science and engineering [20–23]. These advancements found applications in the solution of computationally demanding combustion problems [24–27]. Notably, supervised ML algorithms have gained attention as an alternative approach to predicting the laminar burning velocity (LBV) of various fuels. However, the application of ML for LBV prediction remains limited and requires further investigation.

In one of the early studies, Mehra et al. [28] conducted experiments to measure the LBV of CO and H_2 enriched natural gas under NTP conditions. They developed an Artificial Neural Network (ANN) model based solely on these measurements, which resulted in increased uncertainty in the model's predictive capability. Furthermore, the model's applicability was restricted to mixtures under NTP conditions. Later, Varghese and Kumar [29] devised an empirical model, employing a power-law correlation, to predict the LBV of syngas–air mixtures. The power-law correlation model was constructed through the utilisation of multiple linear regression, with model parameters (temperature and pressure components) being trained using ML methods. The empirical model was calibrated using both experimental data and 1D glass-box model computations. It was reported that the predictions generated by the empirical model exhibited an error margin of under 10%. Subsequently, Malik et al. [30] employed deep neural networks (DNN) to predict the LBV of H_2/air and C_3H_8/air mixtures. They randomly sampled the dataset from available experimental data to ensure sufficient training data. While the model performed well across a wide range of temperature and equivalence ratio conditions, its validation was limited to near atmospheric pressure conditions. Ambritus et al. [31] utilised DNN to estimate the LBV of H_2/air mixtures, employing both experimental and interpolation-based synthetic data for model training. Validation was performed by comparing the results with the Malet correlation. However, the non-homogeneity of the experimental dataset led to lower predictive accuracy, necessitating further experimental measurements. In another study, vom Lehn et al. [32] explored the use of ANN for predicting LBV across various molecular combinations of pure hydrocarbon and oxygenated hydrocarbon fuels. Their dataset encompassed experimental LBV data of 124 fuel compounds and additional data generated through 1D numerical simulations using a detailed chemical kinetic mechanism, amounting to 3,444 data points. It was concluded that ML can be employed for designing new fuels with reasonable prediction accuracy. Eckart et al. [33] confirmed the accuracy of ANN in comparison with other ML models for LBV prediction in H_2/CH_4/air mixtures. The ANN model exhibited comparable performance to the GRI 3.0 mechanism, with a slight reduction in accuracy but significantly lower computational cost. It should be noted that the performance of other ML models can surpass ANN depending on the choice of input parameters and data structure. Later, Wan et al. [34] developed a data-driven ML model using available

experimental data for hydrocarbon (HC) and oxygenated fuels. They employed 5 descriptors calculated from semi-empirical quantum chemistry methods as inputs to the model and evaluated 16 models based on various error metrics (R^2, MAE, RMSE, MSE). Their findings indicated that the Gaussian Process Regression (GPR) algorithm with a squared exponential kernel yielded the best performance. Nevertheless, the model was not validated for high-pressure and high-temperature conditions. More recently, Shahpouri et al. [35] investigated the ML-based prediction of laminar flame speed for low-carbon fuels like NH_3, H_2, CH_3OH, and their combinations. The study employed 1D simulations to generate a substantial LBV database and subsequently trained the models using ANN and Support Vector Machine (SVM) algorithms. While the models claimed to possess predictive capabilities for engine-relevant conditions, the absence of experimental measurements to verify these claims raises uncertainties about their validity at present. Further research and validation are required to assess the performance of these models accurately. Udaybhanu and Reddy [36] used genetic algorithms to optimise ANN weights in predicting the LBV of isooctane/air blends. This method was found to be superior to various other ML algorithms achieving a R^2 of 0.991. Very recently, Üstün et al. [37] applied ML to predict LBV of NH_3/H_2/air mixtures for a wide range of conditions. The performance of a wide range of ML algorithms was comparatively assessed. The GPR and ANN algorithms were found to be more accurate than other tested algorithms. The hyperparameters of the best ML model were optimised and the final model was validated against recent experiments at different conditions. It was also reported that a substantial speed-up in LBV computation time (9,500 to 27,000 times) is achievable with ML models compared to 1D simulations.

Only a few of the studies in the existing literature focus on emerging zero-carbon fuels such as NH_3 and H_2 and their blends that are promising to replace HC fuels. The present work is a continuation of our previous study [37] on predicting the LBV of NH_3/H_2/air mixtures using a machine learning approach. The novelty of the current work lies in the development of an ensemble ML model for the prediction of LBV of poorly studied ternary blends for a wide range of conditions. Moreover, the final ensemble ML model is used to study ternary contours of LBV for all possible $NH_3/CH_4/H_2$ blending ratios with varying T_i, P_i and ϕ where no experiments have been carried out so far. The subsequent sections of this paper are organised into three primary sections. Section 2 presents the methodology, encompassing data collection and data generation procedures employed for training the ML model, the ML model training approach, and the model validation. In Section 3, an exploration of the inter-dependencies among input features is demonstrated, along with a thorough evaluation of the results' validity. Additionally, the ML-based LBV maps are assessed under varying T_i, P_i, and ϕ. Lastly, Section 4 offers conclusive insights into the findings derived from the study, followed by an in-depth discussion on potential future directions of research in this domain.

2. Methodology

2.1. Data analysis

The experimental LBV data for a wide range of fuel mixtures and initial conditions is collected from the literature. Due to some data points acting as outliers, such as extreme pressures or very lean/rich conditions, the training data is bounded by limiting minimum and maximum values. It is worthy of mentioning that the experimental measurements are prone to uncertainties especially near the flammability limits. These uncertainties are especially high (exceeding 20%) for NH_3/air or NH_3 rich flames due to radiation effects [38]. Therefore, any data point with an uncertainty higher than 20% is removed from the training data set to reduce their effects on the model accuracy as outliers. This improves the homogeneity of the training data and eases the data imbalance problem for ML training. Additionally, the equivalence ratio range is decided based on the operability range of $NH_3/CH_4/H_2$/air blends as recently shown by Mashruk et al. [9]. The original and the bounded datasets are given in Table 1.

Table 1
ML model training dataset ranges for available literature data on LBV of NH_3/air, H_2/air, CH_4/air, NH_3/CH_4/air, NH_3/H_2/air, CH_4/H_2/air, and $NH_3/H_2/CH_4$/air mixtures [13–17,39–126].

Measured parameter	Measured range	Training data range
Pressure (bar)	0.07–70	1–10
Temperature (K)	268–756	295–756
Equivalence ratio (ϕ)	0.22–7.15	0.5–1.8
NH_3 content (vol%)	0.0–100.0	0.0–100.0
H_2 content (vol%)	0.0–100.0	0.0–100.0
CH_4 content (vol%)	0.0–100.0	0.0–100.0
LBV (cm/s)	0.98–549	0.98–549
Number of experimental data	4,462	3,846

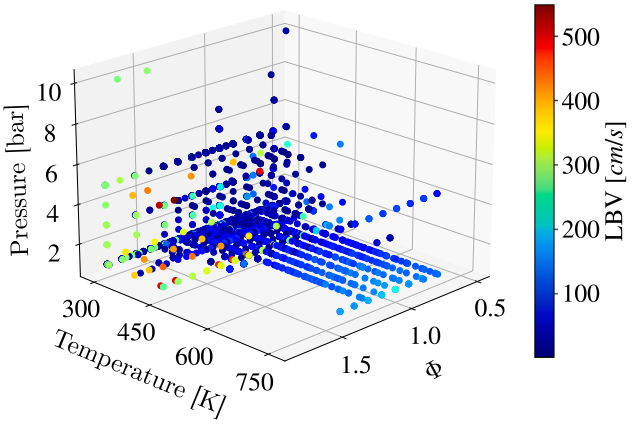

Fig. 1. Distribution of the LBV data over initial temperature, pressure and equivalence ratio.

Even though the training dataset is more homogeneous compared to the original experimental dataset, it should be noted that the majority of the experiments were performed at NTP conditions which skews the distribution of the data. This can clearly be seen in Fig. 1 and should be studied further. In doing so, the distributions of the features in the training dataset are plotted in logarithmic scale in Fig. 2. It is prominent that certain conditions are not well-studied, and some conditions are not studied at all (e.g. $H_2 > 0.6$, $T > 450$ K, and $P > 5$ bar).

Additionally, Fig. 3 shows the box plots of the features to examine their distributions and identify any outliers in the training dataset. The box extends from the first to third quartiles, with the median of the data indicated by the horizontal line within the box. The whiskers extend to the points that are within 1.5 interquartile ranges of the median, and any points beyond this range are considered outliers. The features are standardised to have a mean of 0 and unit variance, i.e., the same scale. While features such as ϕ, NH_3, H_2, and CH_4 show a relatively good distribution, T and P contain undesirable outliers that may negatively affect ML training. These analyses suggest that more data at these underrepresented regions of the training dataset is needed.

The Pearson correlation matrix can be used to examine the relationships between input features and output. It is seen in Fig. 4 that H_2 and LBV have the highest positive correlation. It is well known that the T_i is positively correlated with LBV as seen in Fig. 2. However, it must be noted that the ϕ has almost the same correlation factor. This can be attributed to the increasing trend of LBV with ϕ for H_2-rich mixtures. Furthermore, NH_3 has the highest negative correlation with LBV as expected. One must note that the correlations depend on the fuel combinations, e.g., the correlation coefficients of binary H_2/NH_3/air blends are different than ternary blends [37].

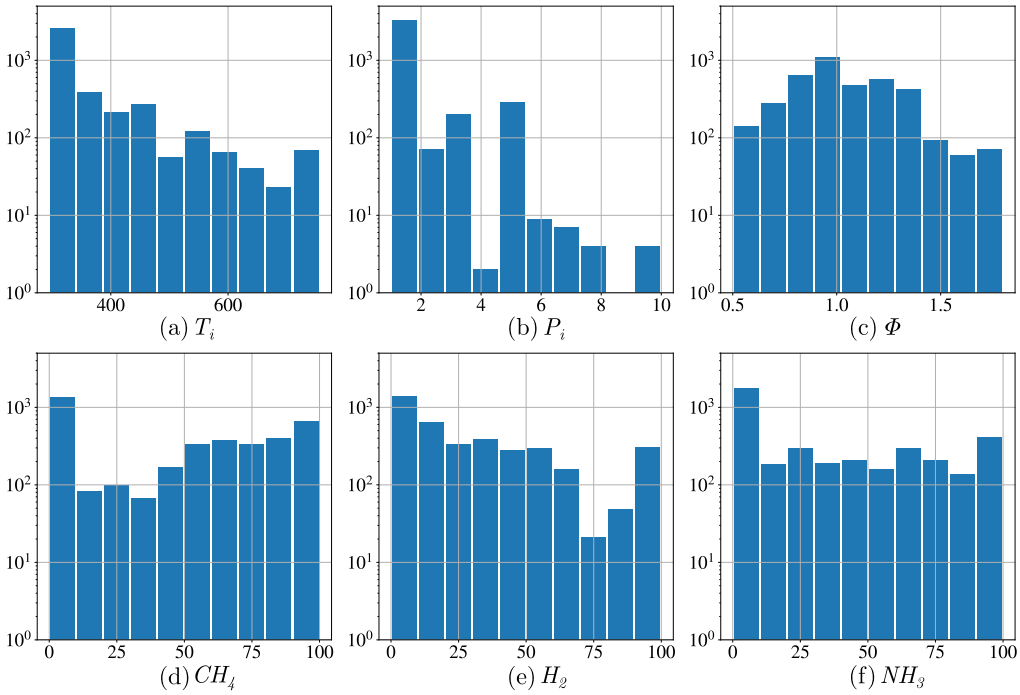

Fig. 2. The distributions of all input features in the experimental dataset; (a) T_i; (b) P_i; (c) ϕ; (d) CH_4; (e) H_2; (f) NH_3.

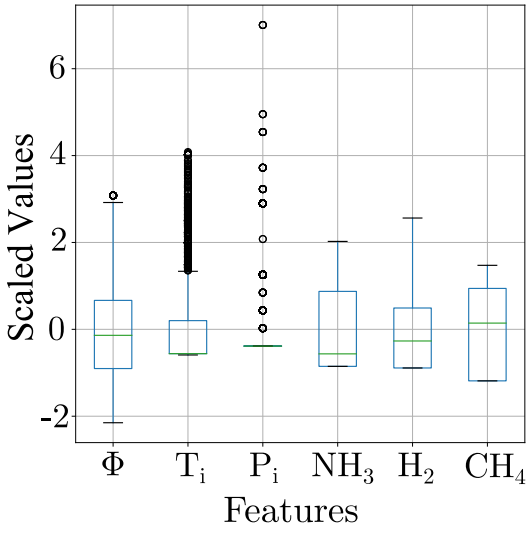

Fig. 3. The box plot demonstrating the distributions and outliers (circles) of all input features in the experimental dataset.

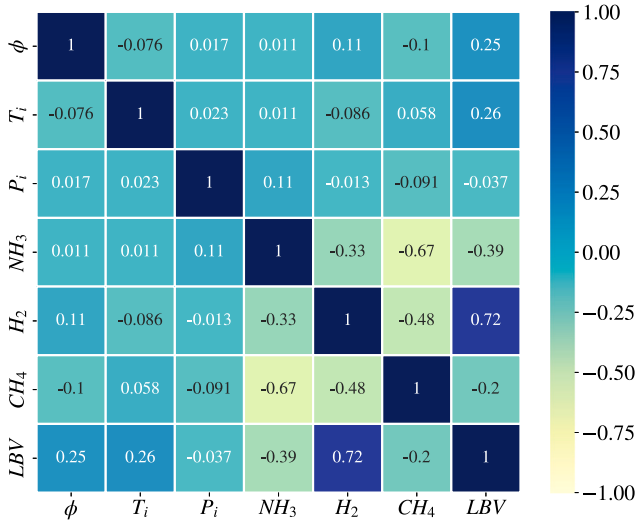

Fig. 4. Pearson correlation matrix based on the experimental dataset.

2.2. Synthetic data generation

It was confirmed in Figs. 2 and 3 that the distribution of the data is non-uniform, imbalanced, and skewed. Skewness in training datasets is usually not a major concern for ML model training as the majority of ML algorithms, except models such as linear regression (since it assumes normally distributed data), can handle skewed training data.

On the other hand, non-uniform data distribution raises generalisability problems as some conditions are under-represented. One way to solve data imbalance is synthetic data generation which uses mechanistic/mathematical models to generate more data points at under-represented conditions. These mathematical models can only be employed if they are validated against experimental data at relevant conditions. In the case of LBV data generation, 1D premixed flame simulations can be employed with a suitable, well-studied chemical kinetic mechanism of choice.

2.2.1. 1D simulations

In this study, the same 1D simulation framework that was established in our previous work [37] is used. 1D freely propagating premixed flame simulations in Cantera [127] are used to generate LBV data points at chosen ranges of conditions. The simulations are carried out with multi-component transport, Soret diffusion, and radiation effects included.

The following conditions are identified as under-represented according to Fig. 3 and targeted for synthetic data generation: P = (4, [6, 10]) bar, ϕ = (0.5, [1.5, 1.8]), T = (450 - 750) K, X_{H_2} = [0.7 – 0.9], X_{CH_4} = [0.1 – 0.5], X_{NH_3} = [0.1 – 0.9]. For the conditions to be simulated, the choice of chemical kinetic mechanism(s) is essential. In

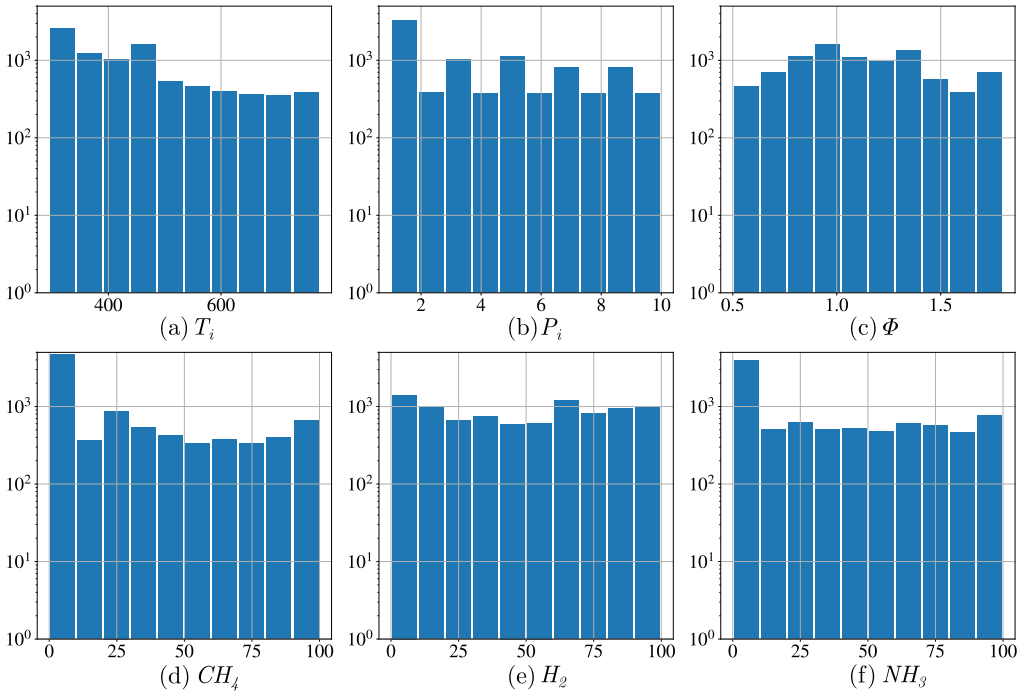

Fig. 5. The distributions of all input features in the hybrid training dataset; (a) T_i; (b) P_i; (c) ϕ; (d) CH_4; (e) H_2; (f) NH_3.

this work, the mechanism by Li et al. [18] is used for simulating ternary $NH_3/H_2/CH_4$/air mixtures since it was tested and reported to be highly accurate by Yasiry et al. [15] and Berwal et al. [13].

In total, an additional 5,088 LBV data points are simulated within specified ranges of conditions to obtain a more uniform distribution for all features which leads to less data imbalance and increased representativeness of the training dataset. The feature distribution of the final training dataset is shown in Fig. 5. It is seen that the uniformity increased substantially due to specifically targeted flame conditions.

2.3. Model validation approach

Model validation holds a central position in ML, serving as a critical assurance for the generalisation capabilities of a model. Employing the cross-validation technique safeguards against the model's reliance on specific training and validation data, ensuring a comprehensive assessment of predictive performance across various scenarios. In this particular investigation, the study adopts the k-fold cross-validation method [128] to validate the model. Within the k-fold cross-validation framework, the dataset is partitioned into k distinct folds, with k set to 10 in this instance, facilitating an iterative training process. Each fold comprises both a training and a validation subset, which varies with each iteration, as depicted in Fig. 6. Consequently, during each iteration, the model's predictive accuracy is tested against the respective validation subset within each individual fold. The overall model error is subsequently determined by averaging the errors across all folds.

2.4. ML algorithms

The choice of ML algorithm to be used for a given regression problem depends on several key factors, including the dataset size, dimensionality, and the complexity of the underlying relationship between the features and the output. In our previous work, 6 ML algorithms and their configurations were tested for the LBV prediction problem. Even though models such as linear regression (LR), regression trees (RT) and ensemble trees (ET) offer better interpretability, they usually cannot describe complex relationships between inputs and output and result in poor predictive performance. Among these algorithms, ANNs and GPR were found the best performers and GPR was chosen for the final model development.

In this section, these algorithms together with the extreme gradient boosting trees (XGBoost) are examined further for the final algorithm and architecture choice. For ML model development, Scikit-learn [129] and TensorFlow [130] libraries are used.

2.4.1. Artificial neural networks

Artificial Neural Networks (ANNs) consist of input, hidden, and output layers which are interconnected by neurons. The aim of the network is to map an N-dimensional input space to an output by learning the complex underlying function governing the output. In this work, a feed-forward ANN is used. In a feed-forward ANN, weights, and biases are initially set to small random values. During forward propagation, input data passes through hidden layers, with each neuron calculating a weighted sum and applying an activation function. The activation function adds non-linearity for complex pattern learning. A loss function measures the difference between the prediction and the ground truth, minimised via back-propagation. Back-propagation updates weights and biases using the gradient descent method. Training involves iterative data input, loss computation, and weight adjustments. After training, inference on new data can be made through forward propagation without weight updates.

2.4.2. Gaussian process regression

In the context of data-efficient regression modelling, Gaussian Process Regression (GPR) stands out as a powerful tool. GPR operates within a probabilistic Bayesian framework, allowing for the effective handling of single-output regression tasks characterised by non-linear relationships [131]. The semi-parametric nature of GPR makes it a more interpretable algorithm compared to fully black-box approximations such as ANNs that have an increasingly large number of parameters depending on the model complexity. Such attributes make it a good choice for constructing intricate non-linear models through the thoughtful design of covariance functions. GPR models are subjected to a rigorous assessment via the computation of the marginal likelihood.

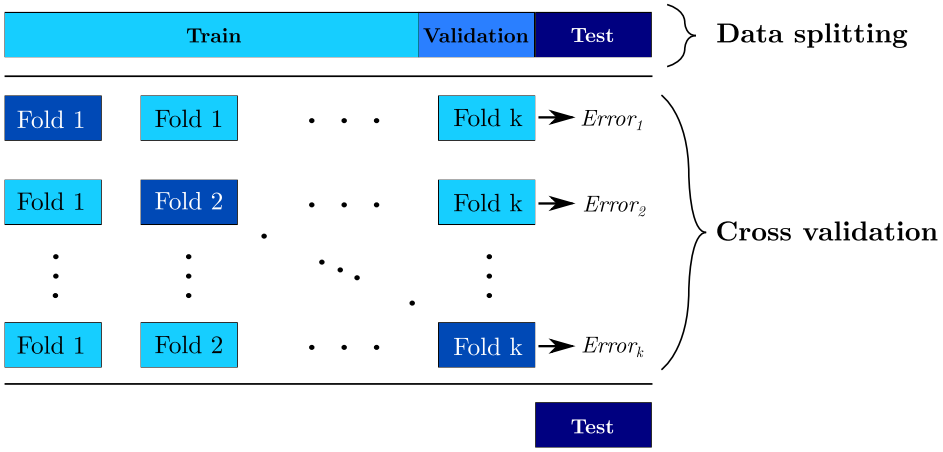

Fig. 6. Schematic of the k-fold cross-validation.

A function, f, can be expressed as follows:

$$y_i = f\left(\boldsymbol{x}_i\right) + \epsilon_i, \tag{1}$$

where X_i $(i = 1, \ldots, n)$ are the set of inputs, y_i $(i = 1, \ldots, n)$ is the output. The ϵ_i term is the noise associated with the observational uncertainty and assumed to have a Gaussian distribution, $\mathcal{N}\left(0; \sigma_n^2\right)$, with a standard deviation of σ_n. The function f can be represented as a Gaussian Process (GP).

A GP is characterised by random variables, with the property that any finite subset of these variables collectively adheres to a joint Gaussian distribution. This process is fully defined by its mean $(\mu(\boldsymbol{x}))$ and covariance functions $(k\left(\boldsymbol{x}, \boldsymbol{x}'\right))$, also known as kernels. Subsequently, for a given process denoted as $f(\cdot)$, GP which incorporates the hyperparameters $\boldsymbol{\theta_\mu}$ and $\boldsymbol{\theta_k}$, can be expressed as follows [132]:

$$f(\cdot) \sim \mathcal{GP}\left(\mu\left(\boldsymbol{x}; \boldsymbol{\theta}_\mu\right), k\left(\boldsymbol{x}, \boldsymbol{x}'; \theta_k\right)\right) \tag{2}$$

The common method for hyperparameter estimation of the covariance function involves maximising the marginal likelihood, which quantifies the likelihood of the observed data given these hyperparameters. The marginal likelihood is computed through integration across the possible function values, denoted as f. If we collect the input data as $\boldsymbol{X}$ and the corresponding output data as $\boldsymbol{Y}$, the natural logarithm of the marginal likelihood can be represented as follows:

$$\begin{aligned}\log(p(\boldsymbol{Y}|\boldsymbol{X}, \boldsymbol{\theta})) = &-\frac{1}{2}(\boldsymbol{Y}-\boldsymbol{\mu})^\top\left(\boldsymbol{K}+\sigma_n^2\boldsymbol{I}\right)^{-1}(\boldsymbol{Y}-\boldsymbol{\mu}) \\ &-\frac{1}{2}\log\left(\left|\boldsymbol{K}+\sigma_n^2\boldsymbol{I}\right|\right)-\frac{n}{2}\log(2\pi)\end{aligned} \tag{3}$$

In this context, the mean vector is denoted as $\boldsymbol{\mu}$, and the covariance matrix is represented by $\boldsymbol{K}$. Consequently, the GP approximation is transformed into an optimisation (maximisation) problem concerning Eq. (3), with a focus on the mentioned hyperparameters. Posterior predictions, under the assumption of a Gaussian error term ϵ_i, can be readily computed using the predictive mean. Furthermore, the quantification of the uncertainty associated with each prediction can be achieved by considering the predictive variance, as discussed by Rasmussen [132].

2.4.3. Extreme Gradient Boosting Trees (XGBoost)

Extreme Gradient Boosting Trees (XGBoost) introduced by Chen and Guestrin [133] within the gradient boosting decision tree (GBDT) framework, form a tree-based ensemble method. The concept involves employing a combination of classification and regression trees (CARTs) to effectively model training data by minimising a regularised objective function. A CART includes a root node, internal nodes, and leaf nodes. The root node initially encompasses all data, which is then divided into internal nodes using binary decision rules, while the leaf nodes represent the final class assignments. In the gradient boosting approach, a sequence of base CARTs is constructed sequentially, with each CART estimator assigned a weight during training to create a robust and accurate ensemble.

Similar to the GPR setting, consider a dataset with m dimensional feature space and n examples $(\mathcal{D} = \left\{(\mathrm{X}_i, y_i)\right\}, (\mathrm{X}_i \in \mathbb{R}^m, y_i \in \mathbb{R}))$. The output to be predicted $(\hat{y}_i)$ can be modelled by XGBoost as follows:

$$\hat{y}_i = \sum_{k=1}^{N} f_k\left(\mathrm{X}_i\right), f_k \in \mathcal{F} \tag{4}$$

where

$$\mathcal{F} = \left\{f(\mathrm{X}) = \omega_{q(\mathrm{X})}\right\}, \left(q : \mathbb{R}^m \to T, \omega \in \mathbb{R}^T\right) \tag{5}$$

In this context, $q_{(X)}$ defines the decision rule that links a given sample to a specific binary leaf index. Furthermore, $\mathcal{F}$ denotes the collection of regression trees, with ω representing the weight assigned to each leaf. Finally, f_k signifies the k_{th} individual tree within this collection, and T signifies the total number of leaves in a tree. The training is carried out by minimising the regularised objective function $\mathcal{L}$ given as:

$$\mathcal{L} = \sum_{i}^{n} l\left(\hat{y}_i, y_i\right) + \sum_{k}^{N} \Omega\left(f_k\right) \tag{6}$$

where y_i is the ground truth target value and l is a differentiable convex loss function. The regularisation term, $\Omega(f_k)$, aims to control model complexity and reduce overfitting and is given by:

$$\Omega(f_k) = \gamma T + \frac{1}{2}\lambda\|\omega\|^2 \tag{7}$$

where $\lambda\|\omega\|^2$ and γ terms are regularisation hyperparameters controlling L2 regularisation (ridge regularisation) and minimum loss reduction required for splitting a new leaf, respectively.

Finally, to minimise the objection function, the greedy function approximation proposed by Friedman [134] is used. The minimisation process, also referred to as gradient boosting, iteratively constructs new decision trees and tries to optimise the objective function to ultimately obtain an accurate ensemble model.

2.5. Model optimisation

2.5.1. ANN

The initial ANN architecture consisted of two hidden layers and 10 neurons for each layer using the rectified linear unit activation function (ReLU). The network is then optimised in terms of the number of hidden layers and neurons for each layer. The ANNs are trained for 2500 epochs, using a batch size of 128. The initial learning rate is set to 10^{-3} with a decay of 3×10^{-4}, and the Adam optimiser is utilised

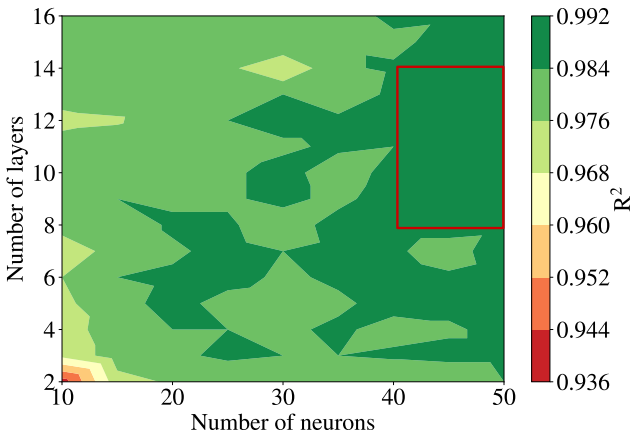

Fig. 7. Accuracy map of neural network architecture in terms of number of neurons per hidden layer and hidden layers represented by R^2 on the test set.

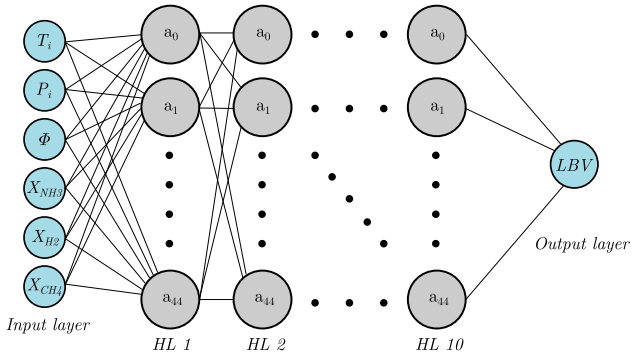

Fig. 8. Optimised neural network structure for the given hybrid training dataset.

for efficient weight updates. The resulting accuracy matrix is shown as a contour in Fig. 7. It is seen that the coefficient of determination, R^2 (Eq. (8)), increases as the number of neurons in each layer increases. Furthermore, the number of layers does not necessarily result in better model accuracy. It can be argued that a network with 40 to 50 neurons and 8 to 14 hidden layers would consistently achieve a high model accuracy as shown with a red box in Fig. 7.

$$R^2 = \frac{\left(\sum_{i=1}^{m}(LBV - \overline{LBV})(LBV - \overline{LBV})\right)^2}{\left(\sum_{i=1}^{m}(LBV - \overline{LBV})\sum_{i=1}^{m}(LBV - \overline{LBV})\right)^2} \tag{8}$$

To maintain model flexibility, i.e., to keep it less complex, we opted for 10 layers and 45 neurons for the final architecture of the ANN. This architecture is illustrated in Fig. 8. To determine an effective train-validation-test split, we monitored the mean absolute loss (MAE) for various combinations of train, validation, and test sets (see Fig. 9) during the training process. The gap between the train and validation loss, known as the generalisation gap, was also considered. It was observed that the generalisation gap was minimised with a 70-15-15 split for train, validation, and test sets, respectively.

2.5.2. GPR

The behaviour of the GPR depends mainly on the choice of kernel. There are a few widely used kernels, but kernels can be designed by combining (e.g. adding or multiplying) existing kernels. In this study, we test squared exponential, radial basis function (RBF), Matérn, and rational quadratic kernels. Each kernel has its own hyper-parameters such as length scale (l), variance (σ^2), scale mixture (α) parameters and so on. These hyper-parameters are optimised during training using L-BFGS-B optimiser.

The optimisation study suggests that the rational quadratic kernel with $l = 0.1$ and $\alpha = 0.5$ reproduces a smooth, expressive posterior mean function.

2.5.3. XGBoost

Even though the performance of the initial XGBoost model is satisfactory, an optimisation study can still be carried out. The hyper-parameters of the XGBoost algorithm are the booster parameters. The optimisation can be carried out by using the HYPEROPT library [135], which utilises Bayesian Optimisation techniques. In our study, we define a range for the hyper-parameters such as the number of estimators, learning rate, and regularisation parameters $\lambda\|\omega\|^2$ and γ. The optimisation study suggests that the optimal number of estimators is 150 and the learning rate is 0.2. It is also observed that the regularisation parameters have low to no effect on the accuracy of the model.

3. Results and discussion

3.1. Model evaluation

The models' performance is systematically evaluated using well-known statistical measures, including the coefficient of determination (R^2), mean absolute error (MAE), root mean square error (RMSE), and the computational speed-up of each model compared to the 1D Cantera model (t_{1D}/t_{ML}) are assessed in Table 2. The definitions of these metrics are given in our previous work [37].

It is seen from Table 2 that the model performances are similar in terms of accuracy. The training and inference speed-up for the GPR model suffers from a relatively larger input vector and dataset size since it has a computational and memory complexity of $O(n^3)$ and $O(n^2)$, respectively [131]. Whereas, XGBoost not only offers the highest accuracy but also achieves the best training and inference times. However, the difference between the train and test R^2 values suggests that the XGBoost model could be slightly overfitted. The difference in train and test error is even more pronounced in the GPR model. Therefore, trusting predictions from only one ML model may be misleading. Thus, a simple ensemble averaging approach is employed here to reduce the bias and over-fitting in the predictions. This approach takes the arithmetic average of the predictions from each model and uses it as the final prediction. The test set error metrics associated with the ensemble-averaged predictions are also included in the Table.

Furthermore, the train and test accuracies can be further examined in Fig. 10. It is seen that the ANN model predictions are more scattered compared to GPR and XGBoost. However, both train and test set predictions are scattered to the same degree, indicating the lack of overfitting. On the other hand, both GPR and XGBoost perform very well on the train set, but, fail to maintain the same level of accuracy for the test set. This is a sign of overfitting and is more prominent in the GPR model which aligns with the error metrics given in Table 2.

3.2. Pressure effects

A complete representation of the LBV space can be given by ternary contours. Ternary contours help visualise the effects of changing three variables on a two-dimensional equilateral triangular. The composition at each point in the contour adds up to 1.0 and the isolines represent the points where LBV stays constant as the composition changes. As an example, the ternary contour for NTP conditions at $\phi = 1.0$ is shown in Fig. 11. The effect of the initial pressure of the flame on the LBV of ternary blends is shown in Fig. 12. Note that each ternary contour contains 20 isolines for better interpretability. It was shown in Fig. 4 that the pressure is weakly inversely proportional to LBV of ternary blends, however, this proportionality is fuel dependent. This proportionality can be easily seen here as the LBV at every point decreases as the pressure is increased. It is also seen that LBV decreases more for the

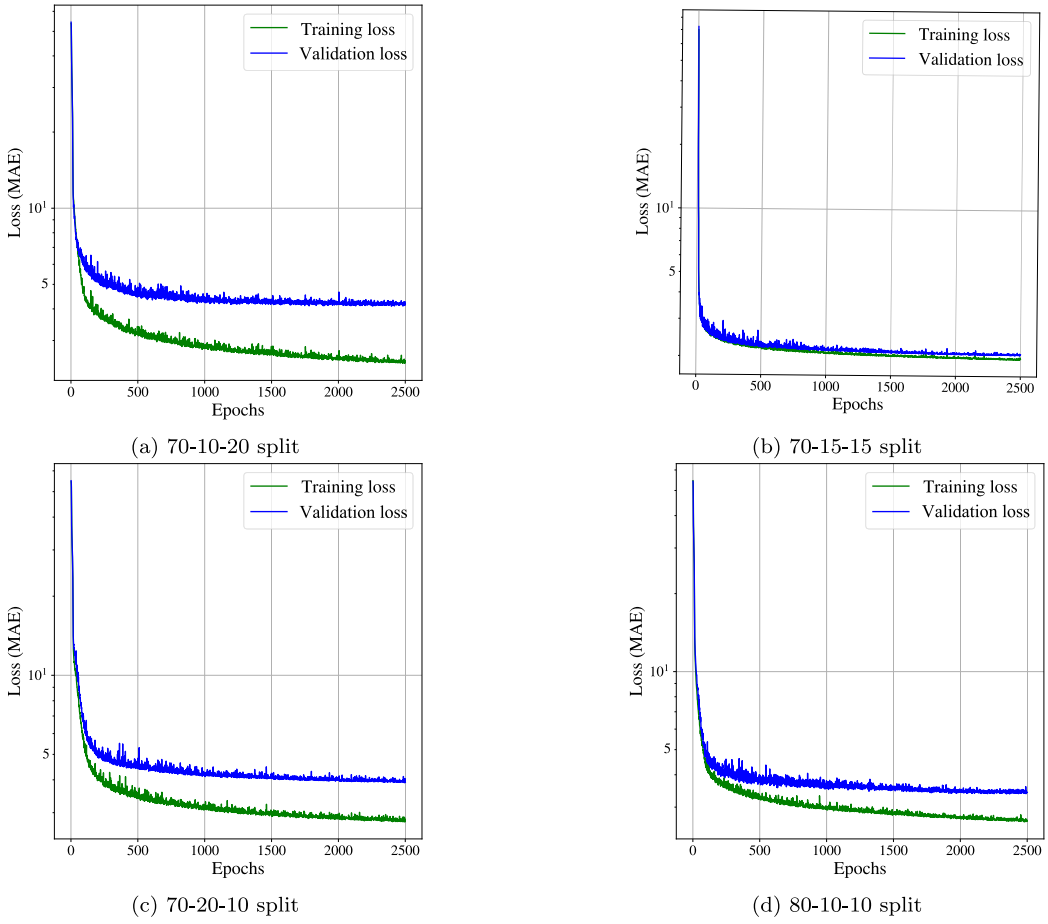

Fig. 9. Train and validation set training loss versus epochs for different train-validation-test splits, (a) 70-10-20 split; (b) 70-15-15 split; (c) 70-20-10 split; (d) 80-10-10 split.

Table 2
Performance evaluation of the ML models.

ML Model	Split set	R^2	MAE (cm/s)	RMSE (cm/s)	Inference speed-up (t_{1D}/t_{ML})
ANN	Train	0.992	2.20	7.99	11,000
	Validation	0.991	2.31	8.23	
	Test	0.991	2.29	8.18	
GPR	Train	0.994	2.01	5.90	8,000
	Validation	0.986	3.75	9.27	
	Test	0.984	4.32	10.62	
XGBoost	Train	0.996	1.95	5.22	28,000
	Validation	0.993	2.17	7.56	
	Test	0.993	2.15	7.83	
Ensemble	Test	0.991	2.92	8.87	8,000

NH_3/CH_4 rich ternary blends as the initial pressure increases showing a higher dependency on pressure.

As it is known, the LBV of CH_4/air is ≈37 cm/s at stoichiometric NTP conditions. Here, the ternary mixture conditions where LBV values are comparable to (± 1 cm/s) to that of CH_4/air are investigated. Table 3 summarises these conditions when the initial temperature (T_i) and ϕ are kept constant and initial pressure (P_i) is varied from 3 to 10 bar. Also, the molar percentages of the species are altered by increments of 5%. It is seen that the NH_3 content does not go above 30% since higher P_i greatly reduces LBV of mixtures with high NH_3 content while its effect on H_2 and CH_4 rich mixtures is not as pronounced. Furthermore, H_2 content increases as P_i increases to obtain desired LBV levels since LBV of H_2 rich mixtures are least affected by pressure.

Table 3
Ternary blends where LBV is comparable to that of CH_4/air at T_i = 300 K and ϕ = 1.0.

P_i (bar)	X_{NH_3}	X_{H_2}	X_{CH_4}	LBV (cm/s)
3	5	35	60	36.01
3	15	40	45	37.44
3	20	40	40	36.41
3	25	45	30	36.19
5	5	50	45	36.54
5	10	55	35	37.09
5	30	65	5	37.37
7	5	65	30	36.68

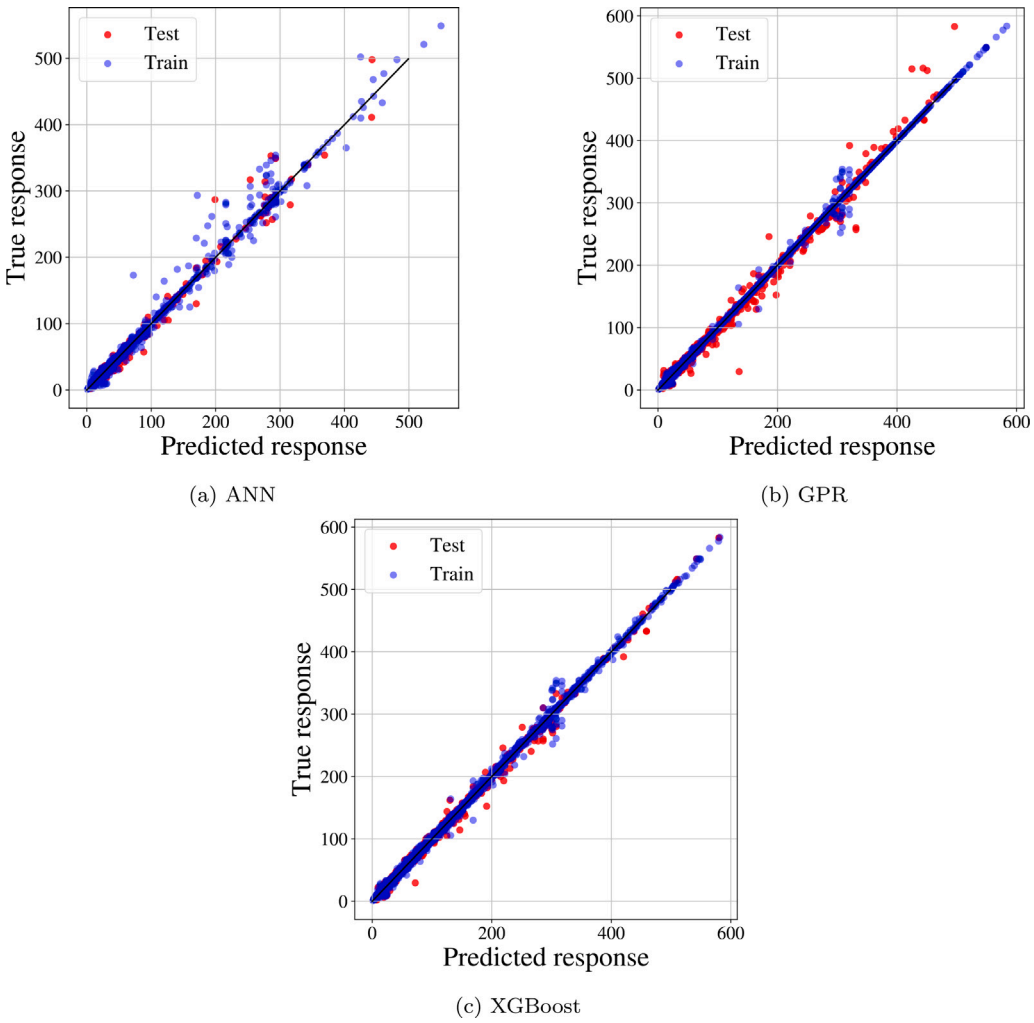

Fig. 10. Predicted versus true LBV values for train and test datasets for all models, (a) ANN; (b) GPR; (c) XGBoost.

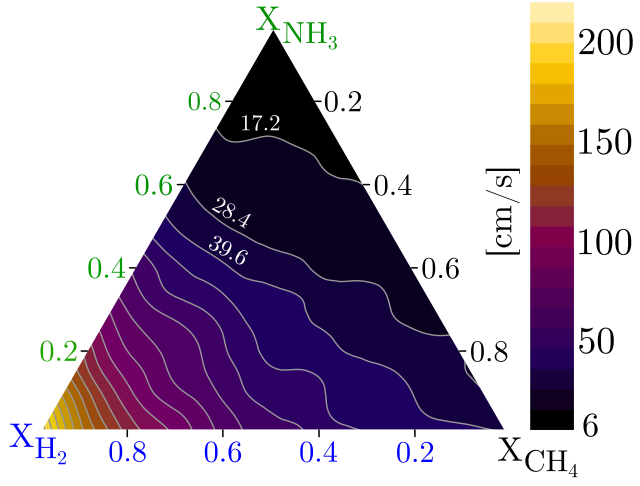

Fig. 11. Ternary contour at NTP conditions and ϕ = 1.0.

3.3. Initial temperature effects

The effect of the initial temperature on the LBV of ternary blends is shown in Fig. 13. The profiles of the isolines dictate a different characteristic compared to initial pressure effects. The initial temperature is directly proportional to the LBV of ternary blends. It is seen that a small addition of H_2 into NH_3 dominant blends greatly enhances the LBV at each flame temperature. Furthermore, it can be seen that LBV changes largely for moderate to high CH_4 contents depending on the overall blending ratios of H_2 and NH_3. However, this effect is much less pronounced for high-pressure conditions as shown in Fig. 12.

Table 4
Ternary blends where LBV is comparable to that of CH_4/air at P_i = 1 bar and ϕ = 1.0.

$T_i(K)$	X_{NH_3}	X_{H_2}	X_{CH_4}	LBV (cm/s)
350	35	10	55	36.07
350	40	15	45	36.59
400	50	20	30	37.94
400	60	30	10	37.97
450	55	10	35	37.10
450	65	20	15	37.15
500	65	5	30	36.68
500	70	10	20	36.46

Table 4 summarises the conditions when P_i = 1 bar, ϕ = 1.0, and T_i is varied from 350 to 500 K with 50 K increments. It is seen that NH_3 rich ternary blends are achievable by increasing T_i. Higher temperatures at these conditions would necessitate even higher NH_3 to limit the LBV to desirable levels.

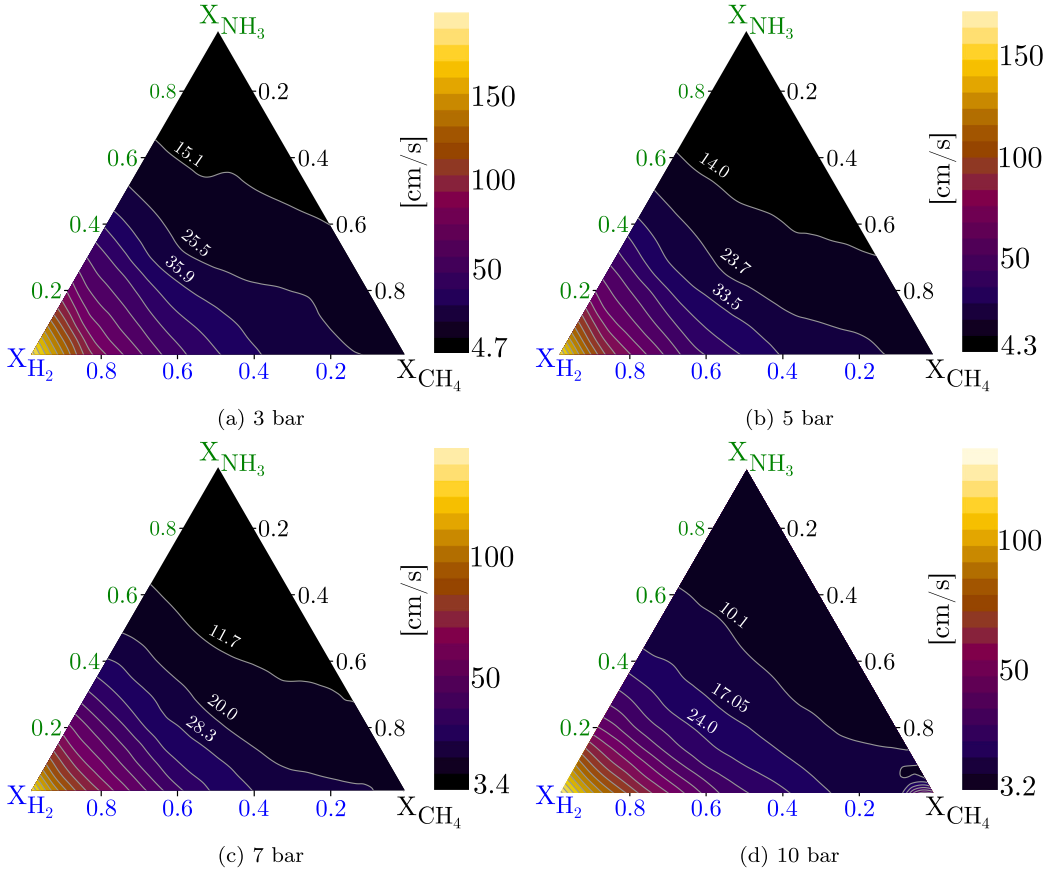

Fig. 12. Ternary blend contour for elevated pressure conditions at T_i = 300 K and ϕ = 1.0; (a) 3 bar; (b) 5 bar; (c) 7 bar; (d) 10 bar.

3.4. Equivalence ratio effects

The effect of the equivalence ratio at NTP conditions is shown in Fig. 14. It is known that the LBV of the majority of the fuels reaches its maximum at slightly fuel-rich conditions ($\phi = 1.0 - 1.1$). However, this is not true in the case of H_2 flames. Therefore, the LBV keeps increasing as the fuel/air ratio is increased in H_2 rich $NH_3/H_2/CH_4$/air blends. On the other hand, LBV of NH_3 and CH_4 rich blends drastically decreases at very rich conditions. It can also be noticed that the LBV profiles are less uniform at very lean conditions, e.g. ϕ = 0.6, when compared to richer conditions. This is an indication of a higher uncertainty involved with both experimentally and numerically determined LBV data. These uncertainties are especially higher for NH_3 rich mixtures since radiation effect is usually not properly accounted for [38].

Similar to Tables 3 and 4, Table 5 summarises the conditions where LBV values between 36 to 38 cm/s can be obtained when ϕ is varied from 0.6 to 1.5 K with 0.3 increments at NTP. Desirable LBV values could not be obtained at very lean conditions (ϕ = 0.6). Fig. 14(a) clearly shows that desirable LBV values occur in a very narrow window of conditions where the mixtures are H_2 rich (> 70% H_2).

Recently, Mashruk et al. [9] observed that a 55/25/20% (vol) $NH_3/H_2/CH_4$/air mixture at NTP and ϕ = 1.2 provides relatively low emissions and good stability. The ensemble model suggests that the LBV value is 21.6 cm/s at these conditions, which is approximately 32% lower than the LBV of CH_4/air mixtures under the same conditions. Similar blends with slightly higher H_2 and/or lower NH_3 content can result in better a LBV with relatively low emissions.

Table 5
Ternary blends where LBV is comparable to the NTP value of CH4/air.

ϕ	X_{NH_3}	X_{H_2}	X_{CH_4}	LBV (cm/s)
0.9	10	25	65	37.91
0.9	20	25	55	36.85
0.9	25	30	45	36.82
0.9	30	40	30	37.39
0.9	35	45	20	37.66
0.9	40	45	15	36.74
0.9	45	45	10	36.03
1.2	30	35	35	37.79
1.2	45	45	10	36.27
1.5	10	60	30	36.68

4. Conclusion

In this work, multiple machine learning (ML) models were applied to predict laminar burning velocity (LBV) of $NH_3/H_2/CH_4$/air mixtures across a wide range of conditions. An extensive literature survey was conducted to gather all available experimental measurements. Then, the experimental dataset was analysed to extract useful insights about the distributions and outliers. Synthetic data was generated at the conditions where LBV measurements are limited using 1D freely propagating premixed flame simulations. This new training dataset was integrated with the original experimental dataset through a hybrid approach to achieve a uniform data distribution across all features. Three ML algorithms, namely Artificial Neural Networks (ANN), Gaussian Process Regression (GPR), and Extreme Gradient Boosting Trees (XGBoost) were trained and optimised. The resulting models were

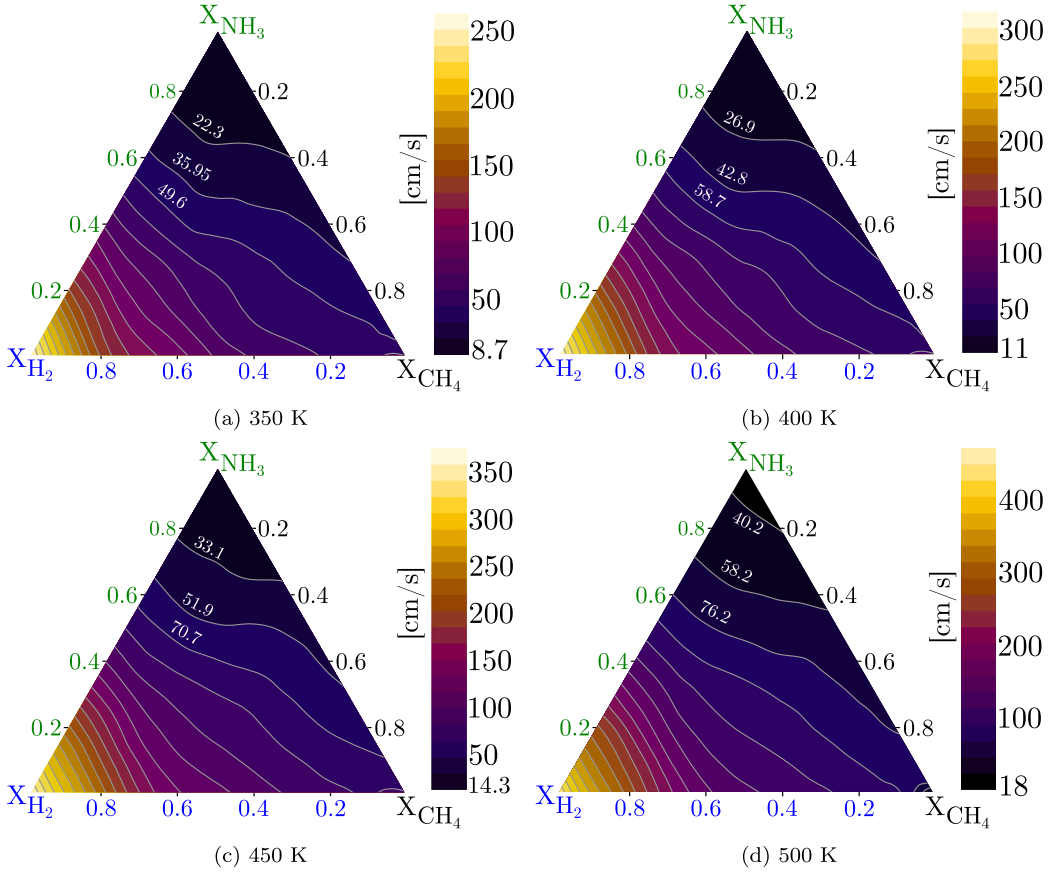

Fig. 13. Ternary blend contour for elevated temperature conditions at P_i =1 bar and ϕ = 1.0; (a) 350 K; (b) 400 K; (c) 450 K; (d) 500 K.

ensembled using simple averaging to manage bias–variance tradeoffs. Then the resulting ensemble model was used to explore the LBV of ternary blends across all mole fractions for a range of pressure, temperature, and equivalence ratios. In summary, the following key findings emerged:

- ML enables the exploration of LBV in poorly studied fuel mixtures, such as $NH_3/H_2/CH_4$/air mixtures.
- The incorporation of synthetic data generated from a chemical kinetic mechanism, along with experimental data, addresses underrepresented conditions and ensures a uniform distribution of the feature vectors.
- XGBoost outperforms ANN and GPR models in all error metrics and inference speed.
- ANNs are capable of achieving a more flexible model with less overfitting when compared to GPR and XGBoost.
- Simple ensemble averaging reduces overfitting and improves model generalisation.
- All models significantly accelerated LBV calculations, reducing computation times by a remarkable factor of at least 8,000 times and up to 28,000 times.

These findings underscore the potential of ML models in the exploration of key combustion features of emerging low-carbon fuels provided that reliable data is available. For future research, the optimisation of the flame conditions of ternary blends in terms of LBV and other fundamental aspects, such as NO_x emissions, will be studied.

CRediT authorship contribution statement

Cihat Emre Üstün: Writing – review & editing, Writing – original draft, Software, Methodology, Data curation, Conceptualization. **Sven Eckart:** Writing – review & editing, Validation, Investigation, Data curation. **Agustin Valera-Medina:** Writing – review & editing, Supervision, Resources, Funding acquisition. **Amin Paykani:** Writing – review & editing, Supervision, Project administration, Methodology, Funding acquisition.

Declaration of competing interest

The authors declare that they have no known competing financial interests or personal relationships that could have appeared to influence the work reported in this paper.

Data availability

The data used in this article is made available in the following link: https://github.com/cihatemreustunn/Ternaryblendsproject This is stated in the Appendix section of the revised manuscript.

Acknowledgement

We gratefully acknowledge financial support by the Engineering and Physical Science Research Council (EPSRC) through grant number EP/T033800/1.

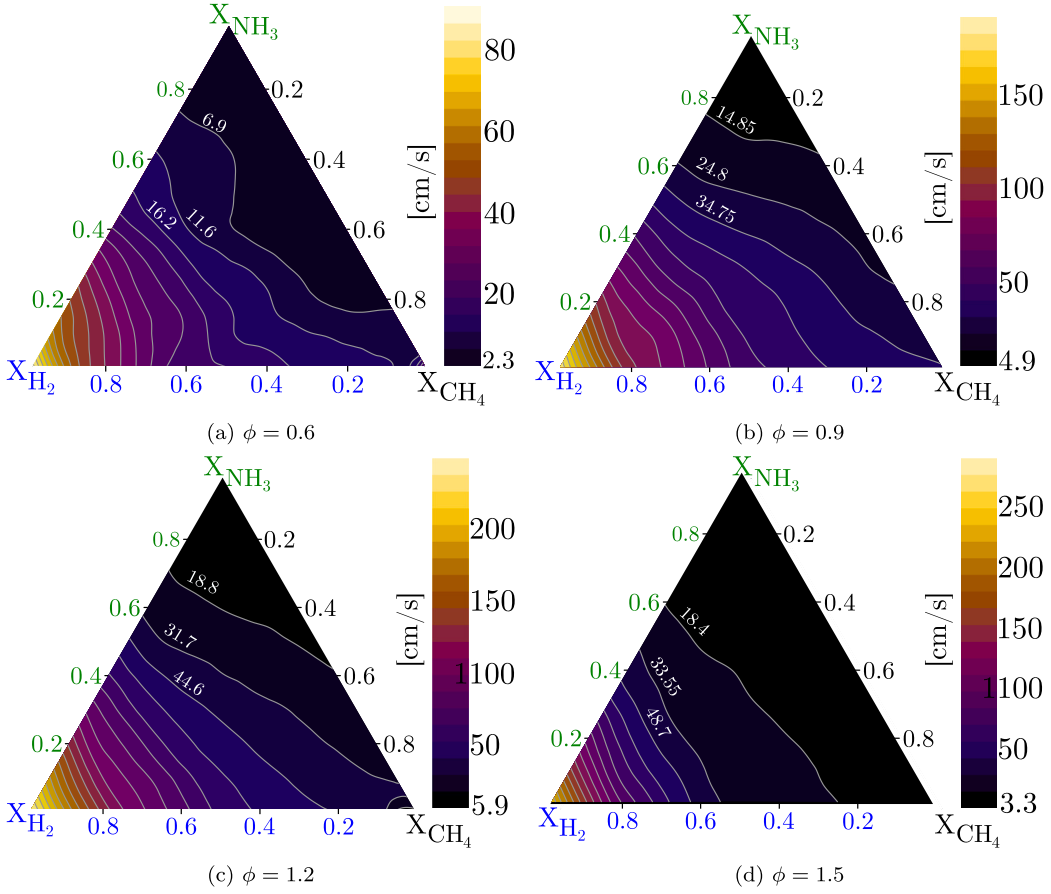

Fig. 14. Ternary blend contour for NTP conditions.

References

[1] Pashchenko D. Ammonia fired gas turbines: Recent advances and future perspectives. Energy 2024;290:130275.

[2] El-Adawy M, Nemitallah MA, Abdelhafez A. Towards sustainable hydrogen and ammonia internal combustion engines: Challenges and opportunities. Fuel 2024;364:131090.

[3] Kobayashi H, Hayakawa A, Somarathne KKA, Okafor EC. Science and technology of ammonia combustion. Proc Combust Inst 2019;37(1):109–33.

[4] Valera-Medina A, Xiao H, Owen-Jones M, David WI, Bowen P. Ammonia for power. Prog Energy Combust Sci 2018;69:63–102.

[5] Valera-Medina A, Amer-Hatem F, Azad A, Dedoussi I, De Joannon M, Fernandes R, et al. Review on ammonia as a potential fuel: from synthesis to economics. Energy Fuels 2021;35(9):6964–7029.

[6] Valera-Medina A, Gutesa M, Xiao H, Pugh D, Giles A, Goktepe B, et al. Premixed ammonia/hydrogen swirl combustion under rich fuel conditions for gas turbines operation. Int J Hydrogen Energy 2019;44(16):8615–26.

[7] Xiao H, Valera-Medina A, Bowen PJ. Modeling combustion of ammonia/hydrogen fuel blends under gas turbine conditions. Energy Fuels 2017;31(8):8631–42.

[8] Valera-Medina A, Pugh D, Marsh P, Bulat G, Bowen P. Preliminary study on lean premixed combustion of ammonia-hydrogen for swirling gas turbine combustors. Int J Hydrogen Energy 2017;42(38):24495–503.

[9] Mashruk S, Vigueras-Zuniga MO, Tejeda-del Cueto M-E, Xiao H, Yu C, Maas U, et al. Combustion features of CH4/NH3/H2 ternary blends. Int J Hydrogen Energy 2022;47(70):30315–27.

[10] Rouwenhorst KH, Castellanos G. Innovation outlook: Renewable ammonia. IRENA; 2022.

[11] Chu H, Feng S, Hong R, Ma X, Qiao F, Chen L. Effects of ammonia addition on soot formation in hydrocarbon fuels combustion: Challenges and prospects. Fuel 2024;360:130569.

[12] Masoumi S, Ashjaee M, Houshfar E. Laminar flame stability analysis of ammonia-methane and ammonia-hydrogen dual-fuel combustion. Fuel 2024;363:131041.

[13] Berwal P, Khandelwal B, Kumar S. Effect of ammonia addition on laminar burning velocity of CH4/H2 premixed flames at high pressure and temperature conditions. Int J Hydrogen Energy 2023.

[14] Berwal P, Kumar S, et al. Laminar burning velocity measurement of CH4/H2/NH3-air premixed flames at high mixture temperatures. Fuel 2023;331:125809.

[15] Yasiry A, Wang J, Zhang L, Dai H, Abdulraheem AA, Shahad HA, et al. Experimental study on the effect of hydrogen addition on the laminar burning velocity of methane/ammonia–Air flames. Appl Sci 2023;13(10):5853.

[16] Okafor EC, Naito Y, Colson S, Ichikawa A, Kudo T, Hayakawa A, et al. Measurement and modelling of the laminar burning velocity of methane-ammonia-air flames at high pressures using a reduced reaction mechanism. Combust Flame 2019;204:162–75.

[17] Shrestha KP, Lhuillier C, Barbosa AA, Brequigny P, Contino F, Mounaïm-Rousselle C, et al. An experimental and modeling study of ammonia with enriched oxygen content and ammonia/hydrogen laminar flame speed at elevated pressure and temperature. Proc Combust Inst 2021;38(2):2163–74.

[18] Li R, Konnov AA, He G, Qin F, Zhang D. Chemical mechanism development and reduction for combustion of NH3/H2/CH4 mixtures. Fuel 2019;257:116059.

[19] Alnasif A, Mashruk S, Shi H, Alnajideen M, Wang P, Pugh D, et al. Evolution of ammonia reaction mechanisms and modeling parameters: A review. Appl Energy Combust Sci 2023;15:100175.

[20] Ahmad S, Shakeel I, Mehfuz S, Ahmad J. Deep learning models for cloud, edge, fog, and IoT computing paradigms: Survey, recent advances, and future directions. Comp Sci Rev 2023;49:100568.

[21] Raschka S, Patterson J, Nolet C. Machine learning in python: Main developments and technology trends in data science, machine learning, and artificial intelligence. Information 2020;11(4):193.

[22] Frank M, Drikakis D, Charissis V. Machine-learning methods for computational science and engineering. Computation 2020;8(1):15.

[23] Shalf J. The future of computing beyond Moore's law. Phil Trans R Soc A 2020;378(2166):20190061.

[24] Zhou L, Song Y, Ji W, Wei H. Machine learning for combustion. Energy AI 2022;7:100128.

[25] Ihme M, Chung WT, Mishra AA. Combustion machine learning: Principles, progress and prospects. Prog Energy Combust Sci 2022;91:101010.

[26] Nguyen H-T, Domingo P, Vervisch L, Nguyen P-D. Machine learning for integrating combustion chemistry in numerical simulations. Energy AI 2021;5:100082.

[27] Aldosari MN, Yalamanchi KK, Gao X, Sarathy SM. Predicting entropy and heat capacity of hydrocarbons using machine learning. Energy AI 2021;4:100054.

[28] Mehra RK, Duan H, Luo S, Ma F. Laminar burning velocity of hydrogen and carbon-monoxide enriched natural gas (HyCONG): An experimental and artificial neural network study. Fuel 2019;246:476–90.

[29] Varghese RJ, Kolekar H, Kumar S. Laminar burning velocities of H2/CO/CH4/CO2/N2-air mixtures at elevated temperatures. Int J Hydrogen Energy 2019;44(23):12188–99.

[30] Malik K, Żbikowski M, Teodorczyk A. Laminar burning velocity model based on deep neural network for hydrogen and propane with air. Energies 2020;13(13):3381.

[31] Ambrutis A, Povilaitis M. Development of a CFD-suitable deep neural network model for laminar burning velocity. Appl Sci 2022;12(15):7460.

[32] vom Lehn F, Cai L, Cáceres BC, Pitsch H. Exploring the fuel structure dependence of laminar burning velocity: A machine learning based group contribution approach. Combust Flame 2021;232:111525.

[33] Eckart S, Prieler R, Hochenauer C, Krause H. Application and comparison of multiple machine learning techniques for the calculation of laminar burning velocity for hydrogen-methane mixtures. Therm Sci Eng Prog 2022;32:101306.

[34] Wan Z, Wang Q-D, Wang B-Y, Liang J. Development of machine learning models for the prediction of laminar flame speeds of hydrocarbon and oxygenated fuels. Fuel Commun 2022;12:100071.

[35] Shahpouri S, Norouzi A, Hayduk C, Fandakov A, Rezaei R, Koch CR, et al. Laminar flame speed modeling for low carbon fuels using methods of machine learning. Fuel 2023;333:126187.

[36] Udaybhanu G, Reddy VM. A hybrid GA-ANN and correlation approach to developing a laminar burning velocity prediction model for isooctane/blends-air mixtures. Fuel 2024;360:130594.

[37] Üstün CE, Herfatmanesh MR, Valera-Medina A, Paykani A. Applying machine learning techniques to predict laminar burning velocity for ammonia/hydrogen/air mixtures. Energy AI 2023;100270.

[38] Faghih M, Valera-Medina A, Chen Z, Paykani A. Effect of radiation on laminar flame speed determination in spherically propagating NH3-air, NH3/CH4-air and NH3/H2-air flames at normal temperature and pressure. Combust Flame 2023;257:113030.

[39] Hayakawa A, Goto T, Mimoto R, Arakawa Y, Kudo T, Kobayashi H. Laminar burning velocity and markstein length of ammonia/air premixed flames at various pressures. Fuel 2015;159:98–106.

[40] Takizawa K, Takahashi A, Tokuhashi K, Kondo S, Sekiya A. Burning velocity measurements of nitrogen-containing compounds. J Hazard Mater 2008;155(1–2):144–52.

[41] Jabbour T, Clodic DF. Burning velocity and refrigerant flammability classification/discussion. ASHRAE Trans 2004;110:522.

[42] Pfahl U, Ross M, Shepherd J, Pasamehmetoglu K, Unal C. Flammability limits, ignition energy, and flame speeds in H2–CH4–NH3–N2O–O2–N2 mixtures. Combust Flame 2000;123(1–2):140–58.

[43] Ronney PD. Effect of chemistry and transport properties on near-limit flames at microgravity. Combust Sci Technol 1988;59(1–3):123–41.

[44] Zakaznov V, Kursheva L, Fedina Z. Determination of normal flame velocity and critical diameter of flame extinction in ammonia-air mixture. Combust Explos Shock Waves 1978;14(6):710–3.

[45] Mei B, Zhang X, Ma S, Cui M, Guo H, Cao Z, et al. Experimental and kinetic modeling investigation on the laminar flame propagation of ammonia under oxygen enrichment and elevated pressure conditions. Combust Flame 2019;210:236–46.

[46] Han X, Wang Z, He Y, Zhu Y, Cen K. Experimental and kinetic modeling study of laminar burning velocities of NH3/syngas/air premixed flames. Combust Flame 2020;213:1–13.

[47] Chen X, Liu Q, Jing Q, Mou Z, Shen Y, Huang J, et al. Flame front evolution and laminar flame parameter evaluation of buoyancy-affected ammonia/air flames. Int J Hydrogen Energy 2021;46(77):38504–18.

[48] Lesmana H, Zhu M, Zhang Z, Gao J, Wu J, Zhang D. Experimental and kinetic modelling studies of laminar flame speed in mixtures of partially dissociated NH3 in air. Fuel 2020;278:118428.

[49] Ji C, Wang Z, Wang D, Hou R, Zhang T, Wang S. Experimental and numerical study on premixed partially dissociated ammonia mixtures. Part I: Laminar burning velocity of NH3/H2/N2/air mixtures. Int J Hydrogen Energy 2022;47(6):4171–84.

[50] Kanoshima R, Hayakawa A, Kudo T, Okafor EC, Colson S, Ichikawa A, et al. Effects of initial mixture temperature and pressure on laminar burning velocity and Markstein length of ammonia/air premixed laminar flames. Fuel 2022;310:122149.

[51] Lee J, Kim J, Park J, Kwon O. Studies on properties of laminar premixed hydrogen-added ammonia/air flames for hydrogen production. Int J Hydrogen Energy 2010;35(3):1054–64.

[52] Kumar P, Meyer TR. Experimental and modeling study of chemical-kinetics mechanisms for H2–NH3–air mixtures in laminar premixed jet flames. Fuel 2013;108:166–76.

[53] Li J, Huang H, Kobayashi N, He Z, Nagai Y. Study on using hydrogen and ammonia as fuels: Combustion characteristics and NOx formation. Int J Energy Res 2014;38(9):1214–23.

[54] Ichikawa A, Hayakawa A, Kitagawa Y, Somarathne KKA, Kudo T, Kobayashi H. Laminar burning velocity and markstein length of ammonia/hydrogen/air premixed flames at elevated pressures. Int J Hydrogen Energy 2015;40(30):9570–8.

[55] Han X, Wang Z, Costa M, Sun Z, He Y, Cen K. Experimental and kinetic modeling study of laminar burning velocities of NH3/air, NH3/H2/air, NH3/CO/air and NH3/CH4/air premixed flames. Combust Flame 2019;206:214–26.

[56] Wang S, Wang Z, Elbaz AM, Han X, He Y, Costa M, et al. Experimental study and kinetic analysis of the laminar burning velocity of NH3/syngas/air, NH3/CO/air and NH3/H2/air premixed flames at elevated pressures. Combust Flame 2020;221:270–87.

[57] Lhuillier C, Brequigny P, Lamoureux N, Contino F, Mounaïm-Rousselle C. Experimental investigation on laminar burning velocities of ammonia/hydrogen/air mixtures at elevated temperatures. Fuel 2020;263:116653.

[58] Gotama GJ, Hayakawa A, Okafor EC, Kanoshima R, Hayashi M, Kudo T, et al. Measurement of the laminar burning velocity and kinetics study of the importance of the hydrogen recovery mechanism of ammonia/hydrogen/air premixed flames. Combust Flame 2022;236:111753.

[59] Li H, Xiao H, Sun J. Laminar burning velocity, Markstein length, and cellular instability of spherically propagating NH3/H2/Air premixed flames at moderate pressures. Combust Flame 2022;241:112079.

[60] Jin B-z, Deng Y-F, Li G-x, Li H-m. Experimental and numerical study of the laminar burning velocity of NH3/H2/air premixed flames at elevated pressure and temperature. Int J Hydrogen Energy 2022;47(85):36046–57.

[61] Chen X, Liu Q, Zhao W, Li R, Zhang Q, Mou Z. Experimental and chemical kinetic study on the flame propagation characteristics of ammonia/hydrogen/air mixtures. Fuel 2023;334:126509.

[62] Zhou S, Cui B, Yang W, Tan H, Wang J, Dai H, et al. An experimental and kinetic modeling study on NH3/air, NH3/H2/air, NH3/CO/air, and NH3/CH4/air premixed laminar flames at elevated temperature. Combust Flame 2023;248:112536.

[63] Tse SD, Zhu D, Law CK. Morphology and burning rates of expanding spherical flames in H2/O2/inert mixtures up to 60 atmospheres. Proc Combust Inst 2000;28(2):1793–800.

[64] Qin X, Kobayashi H, Niioka T. Laminar burning velocity of hydrogen–air premixed flames at elevated pressure. Exp Therm Fluid Sci 2000;21(1–3):58–63.

[65] Kwon O, Faeth G. Flame/stretch interactions of premixed hydrogen-fueled flames: measurements and predictions. Combust Flame 2001;124(4):590–610.

[66] Pareja J, Burbano HJ, Ogami Y. Measurements of the laminar burning velocity of hydrogen–air premixed flames. Int J Hydrogen Energy 2010;35(4):1812–8.

[67] Liu D, MacFarlane R. Laminar burning velocities of hydrogen-air and hydrogen-air steam flames. Combust Flame 1983;49(1–3):59–71.

[68] Wu CK, Law CK. On the determination of laminar flame speeds from stretched flames. In: Symposium (international) on combustion, vol. 20. Elsevier; 1985, p. 1941–9.

[69] Günther R, Janisch G. Measurements of burning velocity in a flat flame front. Combust Flame 1972;19(1):49–53.

[70] Aung K, Hassan M, Faeth G. Effects of pressure and nitrogen dilution on flame/stretch interactions of laminar premixed H2/O2/N2 flames. Combust Flame 1998;112(1–2):1–15.

[71] Lamoureux N, Djebaıli-Chaumeix N, Paillard C-E. Laminar flame velocity determination for H2–air–He–CO2 mixtures using the spherical bomb method. Exp Therm Fluid Sci 2003;27(4):385–93.

[72] Dahoe A. Laminar burning velocities of hydrogen–air mixtures from closed vessel gas explosions. J Loss Prev Process Ind 2005;18(3):152–66.

[73] Huang Z, Zhang Y, Zeng K, Liu B, Wang Q, Jiang D. Measurements of laminar burning velocities for natural gas–hydrogen–air mixtures. Combust Flame 2006;146(1–2):302–11.

[74] Hu E, Huang Z, He J, Jin C, Zheng J. Experimental and numerical study on laminar burning characteristics of premixed methane–hydrogen–air flames. Int J Hydrogen Energy 2009;34(11):4876–88.

[75] Burke MP, Chen Z, Ju Y, Dryer FL. Effect of cylindrical confinement on the determination of laminar flame speeds using outwardly propagating flames. Combust Flame 2009;156(4):771–9.

[76] Kuznetsov M, Kobelt S, Grune J, Jordan T. Flammability limits and laminar flame speed of hydrogen–air mixtures at sub-atmospheric pressures. Int J Hydrogen Energy 2012;37(22):17580–8.

[77] Grosseuvres R, Comandini A, Bentaib A, Chaumeix N. Combustion properties of H2/N2/O2/steam mixtures. Proc Combust Inst 2019;37(2):1537–46.

[78] Dayma G, Halter F, Dagaut P. New insights into the peculiar behavior of laminar burning velocities of hydrogen–air flames according to pressure and equivalence ratio. Combust Flame 2014;161(9):2235–41.

[79] Krejci MC, Mathieu O, Vissotski AJ, Ravi S, Sikes TG, Petersen EL, et al. Laminar flame speed and ignition delay time data for the kinetic modeling of hydrogen and syngas fuel blends. J Eng Gas Turbines Power 2013;135(2).

[80] Sun Z-Y, Li G-X. Propagation characteristics of laminar spherical flames within homogeneous hydrogen-air mixtures. Energy 2016;116:116–27.

[81] Cai X, Wang J, Bian Z, Zhao H, Zhang M, Huang Z. Self-similar propagation and turbulent burning velocity of CH4/H2/air expanding flames: Effect of Lewis number. Combust Flame 2020;212:1–12.

[82] Khan A, Ravi M, Ray A. Experimental and chemical kinetic studies of the effect of H2 enrichment on the laminar burning velocity and flame stability of various multicomponent natural gas blends. Int J Hydrogen Energy 2019;44(2):1192–212.
[83] Morovatiyan M, Shahsavan M, Baghirzade M, Mack JH. Effect of hydrogen and carbon monoxide addition to methane on laminar burning velocity. In: Internal combustion engine division fall technical conference, vol. 59346. American Society of Mechanical Engineers; 2019, V001T02A006.
[84] Eckart S, Krause H. Renewable hydrogen in gas grids, effects on laminar burning velocities. Int J Energy Eng 2018;8:1–9.
[85] Wang Z, Wang S, Whiddon R, Han X, He Y, Cen K. Effect of hydrogen addition on laminar burning velocity of CH4/DME mixtures by heat flux method and kinetic modeling. Fuel 2018;232:729–42.
[86] Lhuillier C, Oddos R, Zander L, Lückoff F, Göckeler K, Paschereit CO, et al. Hydrogen-enriched methane combustion diluted with exhaust gas and steam: Fundamental investigation on laminar flames and NOx emissions. In: Turbo expo: power for land, sea, and air, vol. 50855. American Society of Mechanical Engineers; 2017, V04BT04A054.
[87] Li Z, Cheng X, Wei W, Qiu L, Wu H. Effects of hydrogen addition on laminar flame speeds of methane, ethane and propane: Experimental and numerical analysis. Int J Hydrogen Energy 2017;42(38):24055–66.
[88] Nilsson EJ, van Sprang A, Larfeldt J, Konnov AA. The comparative and combined effects of hydrogen addition on the laminar burning velocities of methane and its blends with ethane and propane. Fuel 2017;189:369–76.
[89] Hu E, Li X, Meng X, Chen Y, Cheng Y, Xie Y, et al. Laminar flame speeds and ignition delay times of methane–air mixtures at elevated temperatures and pressures. Fuel 2015;158:1–10.
[90] Donohoe N, Heufer A, Metcalfe WK, Curran HJ, Davis ML, Mathieu O, et al. Ignition delay times, laminar flame speeds, and mechanism validation for natural gas/hydrogen blends at elevated pressures. Combust Flame 2014;161(6):1432–43.
[91] Morones A, Ravi S, Plichta D, Petersen E, Donohoe N, Heufer A, et al. Laminar and turbulent flame speeds for natural gas/hydrogen blends. In: Turbo expo: power for land, sea, and air, vol. 45691. American Society of Mechanical Engineers; 2014, V04BT04A039.
[92] Okafor EC, Hayakawa A, Nagano Y, Kitagawa T. Effects of hydrogen concentration on premixed laminar flames of hydrogen–methane–air. Int J Hydrogen Energy 2014;39(5):2409–17.
[93] Katharina G, Albin E, Krüger O, Paschereit CO. Burning velocities of hydrogen-methane-air mixtures at highly steam-diluted conditions. In: 4th international conference on jets, wakes and separated flows. 2013.
[94] Moccia V, D'Alessio J. Burning behaviour of high-pressure CH4-H2-air mixtures. Energies 2013;6(1):97–116.
[95] Troshin KY, Borisov A, Rakhmetov A, Arutyunov V, Politenkova G. Burning velocity of methane–hydrogen mixtures at elevated pressures and temperatures. Russ. J. Phys. Chem. B 2013;7:290–301.
[96] Boushaki T, Dhué Y, Selle L, Ferret B, Poinsot T. Effects of hydrogen and steam addition on laminar burning velocity of methane–air premixed flame: experimental and numerical analysis. Int J Hydrogen Energy 2012;37(11):9412–22.
[97] Salzano E, Cammarota F, Di Benedetto A, Di Sarli V. Explosion behavior of hydrogen–methane/air mixtures. J Loss Prev Process Ind 2012;25(3):443–7.
[98] Dirrenberger P, Le Gall H, Bounaceur R, Herbinet O, Glaude P-A, Konnov A, et al. Measurements of laminar flame velocity for components of natural gas. Energy Fuels 2011;25(9):3875–84.
[99] Park O, Veloo PS, Liu N, Egolfopoulos FN. Combustion characteristics of alternative gaseous fuels. Proc Combust Inst 2011;33(1):887–94.
[100] Yan B, Wu Y, Liu C, Yu J, Li B, Li Z, et al. Experimental and modeling study of laminar burning velocity of biomass derived gases/air mixtures. Int J Hydrogen Energy 2011;36(5):3769–77.
[101] Hermanns R, Konnov A, Bastiaans R, De Goey L, Lucka K, Köhne H. Effects of temperature and composition on the laminar burning velocity of CH4+H2+O2+N2 flames. Fuel 2010;89(1):114–21.
[102] Cammarota F, Di Benedetto A, Di Sarli V, Salzano E, Russo G. Combined effects of initial pressure and turbulence on explosions of hydrogen-enriched methane/air mixtures. J Loss Prev Process Ind 2009;22(5):607–13.
[103] Fairweather M, Ormsby M, Sheppard C, Woolley R. Turbulent burning rates of methane and methane–hydrogen mixtures. Combust Flame 2009;156(4):780–90.
[104] Hu E, Huang Z, He J, Zheng J, Miao H. Measurements of laminar burning velocities and onset of cellular instabilities of methane–hydrogen–air flames at elevated pressures and temperatures. Int J Hydrogen Energy 2009;34(13):5574–84.
[105] Miao H, Jiao Q, Huang Z, Jiang D. Measurement of laminar burning velocities and Markstein lengths of diluted hydrogen-enriched natural gas. Int J Hydrogen Energy 2009;34(1):507–18.
[106] Tahtouh T, Halter F, Samson E, Mounaïm-Rousselle C. Effects of hydrogen addition and nitrogen dilution on the laminar flame characteristics of premixed methane–air flames. Int J Hydrogen Energy 2009;34(19):8329–38.
[107] Shy S, Chen Y, Yang C, Liu C, Huang C. Effects of H2 or CO2 addition, equivalence ratio, and turbulent straining on turbulent burning velocities for lean premixed methane combustion. Combust Flame 2008;153(4):510–24.
[108] Braun-Unkhoff M, Kick T, Frank P, Aigner M. An investigation on laminar flame speed as part of needed combustion characteristics of biomass-based syngas fuels. In: Turbo expo: power for land, sea, and air, vol. 47918. 2007, p. 343–52.
[109] Coppens F, De Ruyck J, Konnov AA. Effects of hydrogen enrichment on adiabatic burning velocity and NO formation in methane+ air flames. Exp Therm Fluid Sci 2007;31(5):437–44.
[110] Halter F, Chauveau C, Gökalp I. Characterization of the effects of hydrogen addition in premixed methane/air flames. Int J Hydrogen Energy 2007;32(13):2585–92.
[111] Han P, Checkel MD, Fleck BA, Nowicki NL. Burning velocity of methane/diluent mixture with reformer gas addition. Fuel 2007;86(4):585–96.
[112] Hermanns RTE. Laminar burning velocities of methane-hydrogen-air mixtures. In: Mathematics and Computer Science. Technische Universiteit Eindhoven; 2007, http://dx.doi.org/10.6100/IR630126.
[113] Ilbas M, Crayford A, Yılmaz I, Bowen P, Syred N. Laminar-burning velocities of hydrogen–air and hydrogen–methane–air mixtures: An experimental study. Int J Hydrogen Energy 2006;31(12):1768–79.
[114] Halter F, Chauveau C, Djebaïli-Chaumeix N, Gökalp I. Characterization of the effects of pressure and hydrogen concentration on laminar burning velocities of methane–hydrogen–air mixtures. Proc Combust Inst 2005;30(1):201–8.
[115] Eckart S, Penke C, Voss S, Krause H. Laminar burning velocities of low calorific and hydrogen containing fuel blends. Energy Procedia 2017;120:149–56.
[116] Le Cong T, Dagaut P. Kinetics of natural gas, natural gas/syngas mixtures oxidation and effect of burnt gas recirculation: Experimental and detailed modeling. In: Turbo expo: power for land, sea, and air, vol. 4790. 2007, p. 387–95.
[117] Wu Z, Lv J, Liu X, Wu W, Zhou S, Yan B, et al. Adiabatic laminar burning velocities and NO generation paths of NH3/H2 premixed flames. J Energy Inst 2023;108:101225.
[118] Zitouni S, Brequigny P, Mounam-Rousselle C. Influence of hydrogen and methane addition in laminar ammonia premixed flame on burning velocity, Lewis number and Markstein length. Combust Flame 2023;253:112786.
[119] Wang S, Wang Z, Chen C, Elbaz AM, Sun Z, Roberts WL. Applying heat flux method to laminar burning velocity measurements of NH3/CH4/air at elevated pressures and kinetic modeling study. Combust Flame 2022;236:111788.
[120] Dai H, Wang J, Cai X, Su S, Zhao H, Huang Z. Measurement and scaling of turbulent burning velocity of ammonia/methane/air propagating spherical flames at elevated pressure. Combust Flame 2022;242:112183.
[121] Dai H, Wang J, Cai X, Su S, Zhao H, Huang Z. Lewis number effects on laminar and turbulent expanding flames of NH3/H2/air mixtures at elevated pressures. Proc Combust Inst 2023;39(2):1689–97.
[122] Liang B, Gao W, Zhang K, Li Y. Ammonia-air combustion and explosion characteristics at elevated temperature and elevated pressure. Int J Hydrogen Energy 2023;48(53):20225–37.
[123] Zitouni S, Brequigny P, Mounam-Rousselle C. Turbulent flame speed and morphology of pure ammonia flames and blends with methane or hydrogen. Proc Combust Inst 2023;39(2):2269–78.
[124] Cheng J, Zhang B. Analysis of explosion and laminar combustion characteristics of premixed ammonia-air/oxygen mixtures. Fuel 2023;351:128860.
[125] Berwal P, Solagar S, Kumar S. Experimental investigations on laminar burning velocity variation of CH4+H2+air mixtures at elevated temperatures. Int J Hydrogen Energy 2022;47(37):16686–97.
[126] Alvarez LF, Shaffer J, Dumitrescu CE, Askari O. Laminar burning velocity of Ammonia/Air mixtures at high pressures. Fuel 2024;363:130986.
[127] Goodwin DG, Moffat HK, Speth RL. Cantera: An object-oriented software toolkit for chemical kinetics, thermodynamics, and transport processes. 2018, version.
[128] Stone M. Cross-validatory choice and assessment of statistical predictions. J R Stat Soc Ser B Stat Methodol 1974;36(2):111–33.
[129] Pedregosa F, Varoquaux G, Gramfort A, Michel V, Thirion B, Grisel O, et al. Scikit-learn: Machine learning in python. J Mach Learn Res 2011;12:2825–30.
[130] Abadi M, Barham P, Chen J, Chen Z, Davis A, Dean J, et al. {TensorFlow}: a system for {large-scale} machine learning. In: 12th USeNIX symposium on operating systems design and implementation. 2016, p. 265–83.
[131] Williams CK, Rasmussen CE. Gaussian processes for machine learning, vol. 2, MA: MIT press Cambridge; 2006.
[132] Rasmussen CE. Gaussian processes in machine learning. In: Summer school on machine learning. Springer; 2003, p. 63–71.
[133] Chen T, Guestrin C. Xgboost: A scalable tree boosting system. In: Proceedings of the 22nd acm sigkdd international conference on knowledge discovery and data mining. 2016, p. 785–94.
[134] Friedman JH. Greedy function approximation: a gradient boosting machine. Ann Statist 2001;1189–232.
[135] Komer B, Bergstra J, Eliasmith C. Hyperopt-sklearn: automatic hyperparameter configuration for scikit-learn. In: ICML workshop on autoML, vol. 9. Citeseer Austin, TX; 2014, p. 50.